

Chirality-dependent magnon lifetime in a compensated half-metallic ferrimagnetMariana M. Odashima,^{*} Alberto Marmodoro, Pawel Buczek, Arthur Ernst, and Leonid Sandratskii[†]
Max-Planck-Institut für Mikrostrukturphysik, Weinberg 2, 06120 Halle, Germany

(Received 3 April 2013; published 17 May 2013)

We report a first-principles investigation of magnetic excitations in a compensated half-metallic ferrimagnet using both the adiabatic Heisenberg model and the dynamic spin susceptibility of the electronic system. The combination of half-metallicity and spin compensation of inequivalent magnetic sublattices generates two acoustic magnon modes characterized by linear dispersions with equal spin wave velocities and an asymmetric Landau damping. The difference in the damping is the consequence of the half-metallicity leading to the gap in the energy of the up-to-down electronic spin-flip excitations, whereas down-to-up excitations are gapless. The engineering of the activation energy of the Stoner excitations opens an avenue for the chirality-selective manipulation of the lifetime of magnons.

DOI: [10.1103/PhysRevB.87.174420](https://doi.org/10.1103/PhysRevB.87.174420)

PACS number(s): 75.30.Ds, 75.50.Gg, 75.78.—n

I. INTRODUCTION

The spin of electron can be used to store,¹ process,² and transmit³ information on a nanoscale. While spintronics⁴ aims at controlling spins of single electrons, the emerging field of magnonics⁵ relies on magnons, i.e., the coherent precession of atomic magnetic moments. In both cases the technological progress requires the development of novel materials.

For atomic spin moments coupled via exchange interaction, the magnon frequencies achieve the terahertz regime. At these frequencies the spin waves can hybridize with the continuum of single-particle spin-flip (Stoner) excitations that leads to the damping of the moments' precession. Such mechanism, known as Landau damping,⁶ reduces the magnon lifetimes and propagation length.⁷ New materials with reduced damping are thus under huge demand in magnonics.⁸ In this context we call attention to a class of candidates from spintronics, the half-metals,⁹ which feature one metallic spin channel while the other one is insulating. From the point of view of the magnon spectrum, the ferromagnetic half-metals have been shown to possess an important property: Despite the conducting character of these materials, the Landau damping can be inoperative here due to the gap in the Stoner spectrum.¹⁰

Until now, magnonics is mostly based on ferromagnets, characterized by parallel alignment of atomic moments. Recent experiments have shown that the use of materials with antiparallel oriented magnetic sublattices, like antiferromagnets (AFM) and ferrimagnets, have great potential for ultrafast spin wave control (optomagnonics).¹¹ For instance, the reversal of the polarity of AFM magnons via circularly polarized light,¹² and the optical directioning of the spin wave emission in a ferrimagnet,¹³ were reported. By exploring different magnetic orderings one can enhance the functionality of magnonic devices, enabling, e.g., optically controlled switches. However, to switch the magnetization of a nanostructure on the ultrafast time scale, the damping of the terahertz magnons needs to be controlled.⁷

In this paper we present a study of the lifetimes of magnons in a particular class of materials, known as half-metallic antiferromagnets (HM-AFM). This concept was developed

by de Groot¹⁴ in his pioneer work on half-metallic magnets. HM-AFMs are not conventional antiferromagnets, but a special case of a ferrimagnet with compensated magnetization. Recent reviews on theoretical candidates of HM-AFMs can be found in Refs. 15 and 16. Despite strong research interest from spintronics, the properties of the spin excitations in these materials have not been addressed. The unique combination of features, namely, the gap in only one spin channel, and the full spin compensation of inequivalent magnetic sublattices, make an expectation of unusual properties of the spin excitations well founded. The aim of our work is to explore this gap, taking de Groot's prototype of a half-metallic antiferromagnet, CrMnSb.¹⁴

Before going to the consideration of this complex material, it is useful to recall the fundamentally different properties of spin waves in well-studied cases of ferromagnets and conventional antiferromagnets with two equivalent sublattices. Focusing on the region of small wave vectors \mathbf{q} , the energy of the acoustic magnons in a ferromagnet is quadratic in q and nondegenerate, whereas the energy of the two degenerate AFM magnon modes behaves linearly. Additionally, all ferromagnetic magnons feature the same direction of precession, which can be characterized as a definite chirality, while the pairs of degenerate antiferromagnet magnon modes precess in opposite directions. Also the damping properties are different: A part of the ferromagnetic acoustic branch lies outside the Stoner continuum and does not experience Landau damping, whereas the antiferromagnetic magnons are damped starting from the lowest energies.¹⁷

Our study shows that, similar to a usual AFM, the HM-AFM exhibit two magnon branches with linear dispersion for small q and zero magnon energy in the $q = 0$ limit (Goldstone mode). Despite inequivalence of the sublattices the spin wave velocities of both branches are equal. Interestingly, the magnon damping is asymmetric, depending on the chirality of the magnons. We also show that the disturbance of the spin compensation by electron doping opens a gap at $q = 0$, and changes the initial linear dispersion to quadratic. At the same time, the change of the position of the Fermi level within the half-metallic gap influences the activation energy of the Stoner excitations, and therefore the lifetimes of the magnons.

II. METHODOLOGY

A. Transverse dynamic spin susceptibility

A powerful tool for the first-principles study of the energies and lifetimes of magnons is the calculation of the dynamic transverse spin susceptibility within linear response time-dependent density functional theory.¹⁸ The electronic structure calculations are based on density-functional theory and the Korringa-Kohn-Rostoker multiple scattering method. The numerical implementation has been recently developed by us and applied to the study of various systems.¹⁹

The susceptibility $\chi(\mathbf{r}, \mathbf{r}', \mathbf{q}, \omega)$ relates the external magnetic field B and the induced magnetization m ,

$$m(\mathbf{r}, \mathbf{q}, \omega) = \int_{\Omega} d\mathbf{r}' \chi(\mathbf{r}, \mathbf{r}', \mathbf{q}, \omega) B(\mathbf{r}', \mathbf{q}, \omega), \quad (1)$$

where ω and \mathbf{q} are the frequency and the wave vector of the magnetic field. The vectors \mathbf{r} , \mathbf{r}' belong to the Wigner-Seitz cell Ω . For magnets with a collinear magnetic ground state, the response to the infinitesimal transverse magnetic field (i.e., field parallel to the xy plane) is also transverse.²⁰

The calculational procedure consists of two steps. First, the dynamic transversal Kohn-Sham (KS) susceptibility

$$\begin{aligned} \chi_{\text{KS}}(\mathbf{r}, \mathbf{r}', \mathbf{q}, \omega) = & \sum_{\mathbf{k} \in \Omega_{\text{BZ}}} \sum_{nn'} (f_{n\mathbf{k}-\mathbf{q}}^{\uparrow} - f_{n'\mathbf{k}}^{\downarrow}) \\ & \times \frac{\psi_{n\mathbf{k}-\mathbf{q}}^{\uparrow}(\mathbf{r}') \psi_{n\mathbf{k}-\mathbf{q}}^{\uparrow}(\mathbf{r})^* \psi_{n'\mathbf{k}}^{\downarrow}(\mathbf{r}) \psi_{n'\mathbf{k}}^{\downarrow}(\mathbf{r}')^*}{\omega - (\epsilon_{n'\mathbf{k}}^{\downarrow} - \epsilon_{n\mathbf{k}-\mathbf{q}}^{\uparrow}) + i0^+} \end{aligned} \quad (2)$$

is evaluated. Here \mathbf{k} , \mathbf{k}' denote crystal momenta belonging to the first Brillouin zone (Ω_{BZ}); $\psi_{n\mathbf{k}}^{\sigma}$ stands for the electronic Bloch state of band n , and $\epsilon_{n\mathbf{k}}^{\sigma}$ and f are its corresponding energy and occupation. The 0^+ symbol denotes the use of the retarded quantities.

The imaginary part of the KS susceptibility gives the spectral density of the Stoner excitations, i.e., single-electron spin flips. For positive frequencies, only electronic transitions between occupied ($f = 1$) spin-up states with crystal momentum $\mathbf{k} - \mathbf{q}$ and empty ($f = 0$) spin-down states with momentum \mathbf{k} contribute to the imaginary part of the KS susceptibility. For negative frequencies, the contribution comes from the Stoner transitions of opposite direction. However, the KS susceptibility does not give the actual magnetic response of the system since the induced spin magnetization alters the exchange-correlation (xc) potential experienced by electrons, and this additional field is not taken into account in χ_{KS} .

To obtain the actual physical response one needs to solve the Dyson equation giving the enhanced (interacting) transverse magnetic susceptibility χ :

$$\begin{aligned} \chi(\mathbf{r}, \mathbf{r}', \mathbf{q}, \omega) = & \chi_{\text{KS}}(\mathbf{r}, \mathbf{r}', \mathbf{q}, \omega) \\ & + \int d\mathbf{r}_1 \chi_{\text{KS}}(\mathbf{r}, \mathbf{r}_1, \mathbf{q}, \omega) K_{\text{xc}}(\mathbf{r}_1) \chi(\mathbf{r}, \mathbf{r}', \mathbf{q}, \omega). \end{aligned} \quad (3)$$

The exchange-correlation kernel K_{xc} accounts for the change of the effective KS potential, and is based on our work on the adiabatic (i.e., frequency-independent) local density approximation.^{10,18} The imaginary part of the enhanced sus-

ceptibility provides information on their energies and lifetimes. In the matrix form, the solution of the Dyson equation can be written as

$$\chi = (\mathbb{I} - \chi_{\text{KS}} K_{\text{xc}})^{-1} \chi_{\text{KS}}. \quad (4)$$

The singularities of the enhanced susceptibility can have two sources: the χ_{KS} Stoner transitions and the zeros of the $\mathbb{I} - \chi_{\text{KS}} K_{\text{xc}}$ term. The step from the noninteracting to the enhanced susceptibility results in a remarkable property where energy absorption can now take place for frequencies outside the Stoner continuum. This manifests in the presence of collective spin wave excitations or magnons.

B. Mapping onto the Heisenberg Hamiltonian

The study of spin waves in itinerant-electron magnets is traditionally based on the adiabatic treatment of magnetic degrees of freedom, which maps the system onto an effective Heisenberg Hamiltonian of atomic moments:

$$H = -\frac{1}{2} \sum_{\mathbf{R}\mathbf{R}'} J_{\mathbf{R}\mathbf{R}'} \mathbf{e}_{\mathbf{R}} \cdot \mathbf{e}_{\mathbf{R}'}, \quad (5)$$

where $\mathbf{e}_{\mathbf{R}}$ is the unit vector in the direction of the atomic spin moment at site \mathbf{R} , and $J_{\mathbf{R}\mathbf{R}'}$ are the pair exchange interactions parameters.

In our first-principles calculations, the exchange interactions $J_{\mathbf{R}\mathbf{R}'}$ are obtained via magnetic force theorem, i.e., by the estimation of the energies of small spin rotations as described in Refs. 21 and 22. We also evaluate effective sublattice exchange parameters, given by the sum of the exchange interactions of a given atom at site \mathbf{R}_i of sublattice i with all other atoms of this sublattice:

$$J_i = \sum_{\mathbf{R}_i(\mathbf{R}_i - \mathbf{R}_j \neq 0)} J_{\mathbf{R}_i \mathbf{R}_j} \quad (\text{intrasublattice}), \quad (6)$$

or with all atoms of another sublattice j ,

$$J_{ij} = \sum_{\mathbf{R}_i} J_{\mathbf{R}_i \mathbf{R}_j} \quad (\text{intersublattice}). \quad (7)$$

In the following section we derive the spin wave dispersion relation in the Heisenberg framework for a general two-sublattice ferrimagnet, and consider the special case of the compensated ferrimagnet. Next, we perform *ab initio* adiabatic calculations in the half-metallic compensated ferrimagnet CrMnSb. We remark that the adiabatic treatment neglects Stoner excitations and gives no information about lifetimes.

III. RESULTS

A. Density of states of a half-metallic compensated ferrimagnet: CrMnSb

In Fig. 1 we show the density of states of half-Heusler CrMnSb. The half-metallic gap is associated with the strong hybridization²³ between 3d states of Cr and Mn sublattices, while Sb stabilizes the $C1_b$ structure.²⁴ From the viewpoint of the electronic structure, there is an important difference between an antiferromagnet with two equivalent sublattices and a ferrimagnet with inequivalent magnetic sublattices. In the former the electronic states are spin degenerate,¹⁷ and

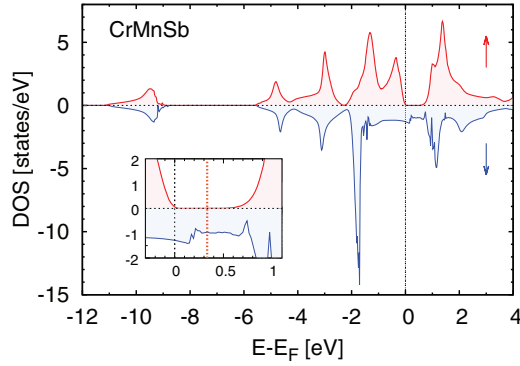


FIG. 1. (Color online) Electronic density of states of the half-metallic CrMnSb, a half-Heusler alloy. Details around the Fermi level are depicted in the inset. A vertical thick dotted line in the inset illustrates a shift of the Fermi level with simulated doping resulting in the change of the activation energy of Stoner excitations (see discussion in the last section of the paper).

the half-metallic gap cannot form. On the other hand, in a ferrimagnet the electronic structures of up and down electrons are different (Fig. 1). The calculated values of the atomic spin moments are $m_{\text{Cr}} = 2.71 \mu_B$ and $m_{\text{Mn}} = -2.75 \mu_B$, with a small positive moment of the Sb atom and interstitial region. We have chosen the direction of the Cr moment as the reference of the spin-quantization axis. Note that the Fermi level lies at the lower edge of the half-metallic gap in the spin-up channel. This feature is important for the understanding of the lifetime properties of the spin wave excitations obtained in the calculation of dynamic susceptibility.

B. Adiabatic spin waves within the Heisenberg model

For deeper understanding of the results of first-principles calculations, it is instructive to first study analytically the spin waves in a compensated ferrimagnet within the framework of the Heisenberg model [Eq. (5)]. We consider a crystal with two inequivalent magnetic atoms in the unit cell, forming two sublattices with the antiparallel atomic moments: S_1 (up) and $-S_2$ (down). Using the Landau-Lifshitz equation to describe the spin dynamics,²⁵ the frequencies $\omega_{\pm}(\mathbf{q})$ of the magnon excitations can be found as the eigenvalues of the following matrix:

$$\begin{pmatrix} \Omega_1(\mathbf{q}) - \frac{2}{S_1} J_{12}(\mathbf{0}) & -\frac{2}{S_1} J_{12}(\mathbf{q}) \\ \frac{2}{S_2} J_{12}(\mathbf{q})^* & -\Omega_2(\mathbf{q}) + \frac{2}{S_2} J_{12}(\mathbf{0}) \end{pmatrix}, \quad (8)$$

where $\Omega_n(\mathbf{q}) = (2/S_n)[J_{nn}(\mathbf{0}) - J_{nn}(\mathbf{q})]$, $n = 1, 2$, is the dispersion of the ferromagnetic magnons that would propagate in each of the sublattices in the absence of the intersublattice coupling $J_{12}(\mathbf{q})$. We cast $J_{nm}(\mathbf{q})$ as

$$J_{nm}(\mathbf{q}) = \sum_{\mathbf{R}} J_{nm}(\mathbf{R}) e^{-i\mathbf{q} \cdot \mathbf{R}}, \quad (9)$$

where the summation proceeds over lattice vectors \mathbf{R} . $J_{nm}(\mathbf{R})$ stands for the Heisenberg exchange interaction between moments on sublattices n and m in the primitive cells separated by vector \mathbf{R} . The dispersions $\omega_{\pm}(\mathbf{q})$ of two branches of magnon

excitations read

$$\omega_{\pm}(\mathbf{q}) = \Delta_{\pm} + D_{\pm}(\mathbf{q}) \pm \sqrt{[\Delta_{\pm} - D_{\pm}(\mathbf{q})]^2 - C(\mathbf{q})}, \quad (10)$$

where $\Delta_{\pm} = J_{12}(\mathbf{0})(S_1 \pm S_2)/(S_1 S_2)$, $D_{\pm}(\mathbf{q}) = \frac{\Omega_1(\mathbf{q}) \pm \Omega_2(\mathbf{q})}{2}$, and $C(\mathbf{q}) = 4|J_{12}(\mathbf{q})|^2/(S_1 S_2)$. In the compensated case ($S_1 = S_2 = S$) the frequencies of both branches vanish for $q = 0$ and assume in the region of small q the form

$$\omega_{\pm}(q) = \pm cq + d_{\pm} q^2 + O(q^3), \quad (11)$$

where $d_{\pm} q^2$ is the quadratic term in the Taylor expansion of $D_{\pm}(\mathbf{q})$, and c is a complex function of the intra- and intersublattice exchange interactions. The signs of the frequencies in Eq. (10) determine the chirality of the magnons and correspond to different directions of the precession.

As mentioned earlier, similar to AFMs²⁶ we obtain two spin wave branches with linear q dependence and energy tending to zero in the $q \rightarrow 0$ limit. The spin wave velocities ($\pm c$) of both branches are of equal magnitude. However, unlike the AFM case, the branches are not equivalent ($\omega_{+} \neq -\omega_{-}$), and there is no symmetry operation that transforms one magnon mode into the other. In the small- q region [Eq. (11)], the symmetry of the branches is broken by the quadratic term proportional to d_{\pm} . In an AFM, $D_{\pm}(\mathbf{q}) = 0$ and therefore d_{\pm} vanishes. For a compensated ferrimagnet, despite equal magnetic moments of the two sublattices, the intrasublattice exchange interactions are different ($\Omega_1 \neq \Omega_2$), resulting in nonzero d_{\pm} . Interestingly, the coefficient d_{\pm} simply amounts to the difference of the spin wave stiffness constants of decoupled ferromagnetic sublattices, and is entirely determined by the intrasublattice exchange parameters.

In the calculations discussed below we also simulate electron doping, which destroys the spin compensation. In the case of uncompensated moments the small- q dispersion of Heisenberg magnons given by Eq. (10) changes qualitatively in two respects. First, for both branches the leading q term becomes quadratic. Second, one of the branches develops an energy gap equal to $2\Delta_{\pm}$, depending on the intersublattice coupling, whereas the other branch remains gapless giving rise to the Goldstone mode. In Fig. 2 we present the first-principles results for the Heisenberg's magnons in CrMnSb, clearly showing all the above features.

C. Spin wave dispersion and lifetimes from dynamic spin susceptibility

Next, we turn to the discussion of first-principles calculations of the spin excitations in CrMnSb. The solid lines in Figs. 2(a) and 2(b) correspond to the frequencies of adiabatic magnons calculated with the use of the Heisenberg model. The inequivalence of the two magnetic sublattices is reflected in the difference of effective sublattice exchange parameters [Eq. (6)]: $J_{\text{Cr}} = 69$ meV and $J_{\text{Mn}} = 12$ meV. The leading intrasublattice exchange interactions are ferromagnetic for both Cr and Mn, while the effective intersublattice exchange interaction [Eq. (7)] is antiferromagnetic ($J_{\text{Cr-Mn}} = -225$ meV), with a much larger magnitude due to the shorter interatomic distance.

Points in Figs. 2(a) and 2(b) correspond to spin waves obtained from dynamic susceptibility calculations. In the insets

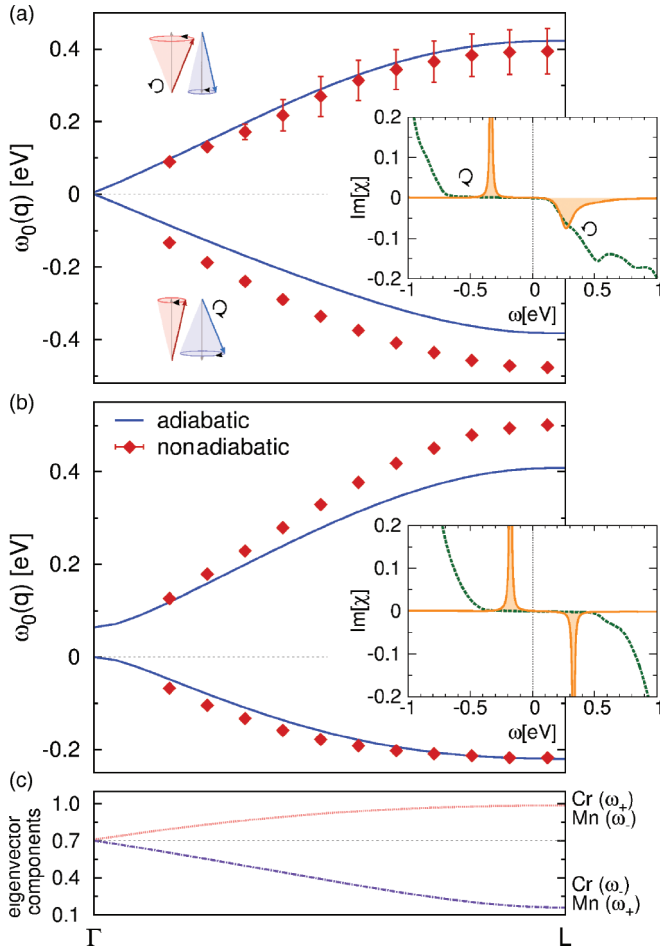


FIG. 2. (Color online) (a) Magnon spectra obtained through Heisenberg adiabatic dynamics (solid curves), and from the dynamic magnetic susceptibility (points) for CrMnSb. The error bars correspond to the inverse lifetimes. The inset presents the spectral densities of spin wave (solid line) and Stoner (broken line) excitations for wave vector $\mathbf{q} = (0.25, 0.25, 0.25)$ corresponding to the center of the ΓL interval. (b) The same as (a) but for electronically doped CrMnSb. (c) The components of the normalized magnon eigenvectors for both magnon branches of the compensated ferrimagnet [(a)]. The upper line shows the deviation from the ground-state direction of the Cr moment in the positive-chirality branch and of the Mn moment in the negative-chirality branch. For the lower line, the atomic assignment to the magnon branches is opposite.

we show spectral densities of the enhanced and unenhanced susceptibilities for one value of the wave vector. The peaks of the enhanced susceptibility correspond to the spin wave excitations: Their position determines the energy of the magnon and their width the inverse lifetime. The spectral density of the Stoner excitations, given by χ_{KS} , is shown as broken lines in the insets. At the frequencies where it is zero, the magnon peaks have the form of a δ function and feature infinite lifetime (filled narrow peaks in the insets). On the other hand, nonzero density of the Stoner transitions at the energy of the magnon leads to Landau damping, reflected in the increased width of the peak [see inset of Fig. 2(a)]. The error bars in Fig. 2(a) denote full widths at the half maximum (FWHM) of the peaks.

A remarkable result is the strong difference in the damping properties of the two modes. While the negative-frequency branch remains undamped up to the Brillouin zone boundary, the magnons of the other branch are substantially damped past the middle of the ΓL interval. For instance, the FWHM at the edge of the BZ zone is 100 meV. This asymmetry is a consequence of the half-metallic character of the electronic structure. Since the system has a gap in the spin-up channel (cf. Fig. 1), there are no low-energy Stoner transitions from spin-down states to spin-up states, while the up-to-down transitions remain practically gapless due to the position of the Fermi level just at the bottom of the half-metallic gap. This property is the origin of the dependence of the magnon lifetime on its chirality: The magnons of negative chirality (ω_-) cannot decay via Landau mechanism and those of positive chirality (ω_+) are damped.

The analytic continuation procedure precludes determination of magnon frequencies from the dynamic susceptibility in the long wavelength limit.¹⁷ This is the reason why the results of the dynamic calculation are given starting from $q = 0.08$. The magnon energies obtained from the dynamic susceptibility are in good agreement with the results of adiabatic calculations. The difference between the two approaches can be traced back to the influence of finite lifetime effects and a systematic error in the determination of Heisenberg exchange parameters with the magnetic force theorem approach.²⁷

It is instructive to characterize the magnons from their origin in the Cr and Mn sublattices. In each magnon state, all atomic moments precess with one single chirality and one single frequency, but with different amplitudes. The values of the deviations of the precessing moments from the ground state direction are given by the eigenvectors of matrix (8). In Fig. 2(c) we show the components of the normalized eigenvectors as a function of q for the case of the compensated system. Each line gives the deviation of a certain type of atomic moment in a given branch. For $q = 0$ the deviations of the moments of both sublattices are equal, as expected for the uniform Goldstone mode. With increasing q the difference of the deviations monotonously increases. At the zone boundary the deviation of the moments of one of the sublattices is much larger than for the other. On this basis the branch of positive chirality can be characterized as “Cr type” while the mode of negative chirality as “Mn type.”

The properties of the spin excitations of half-metals are significantly affected by the change of the activation energy of the Stoner excitations that can be achieved, for instance, through doping. We have simulated doping by increasing the electron number of all three elements by $0.2e$. This procedure shifts the Fermi level to the middle of the gap (cf. Fig. 1). The compensation of the spin moments is lost since additional electrons result in a negative total moment.

The disturbance of the spin compensation leads to the opening of a gap at $q = 0$ between the two spin wave branches [Fig. 2(b)]. The most important change pertains, however, to the lifetimes. Since the Fermi level reaches now the middle of the half-metallic gap, both up-to-down and down-to-up Stoner transitions develop comparable activation energies, as evident from the dashed lines in the inset of Fig. 2(b). The absence of the Stoner transitions at the spin wave energies makes Landau damping inoperative for both branches.

IV. CONCLUSIONS

In summary, we study the dispersion and lifetimes of spin wave excitations in a half-metallic compensated ferrimagnet, using both the Heisenberg adiabatic and the electronic dynamic susceptibility approaches. Half-metallicity is a natural source of protection against magnons attenuation, and we show that HM-AFMs exhibit unique excitation properties, combining virtues of antiferromagnets and ferromagnets. Due to inequivalence of the sublattices, we observe an asymmetric damping of the magnon branches that can be useful in the design of magnonic devices with selective use of spin wave branches. The damping can be efficiently manipulated by influencing the position of the Fermi level within the half-metallic gap. On the practical side, there

are several challenges ahead. Further efforts are needed to synthesize and experimentally study half-metallic antiferromagnets. The Heusler alloys are good candidates for the search for new half-metallic antiferromagnets due to typically high magnetic critical temperature and compatibility with semiconductor technology.^{16,23} We hope that our findings will further stimulate the research on this promising class of materials.

ACKNOWLEDGMENTS

Funding from the Deutsche Forschungsgemeinschaft is acknowledged by A.M. and A.E. (DFG priority program SPP 1538 “Spin Caloric Transport”).

*odashima@mpi-halle.mpg.de

†lsandr@mpi-halle.de

¹J. Åkerman, *Science* **308**, 508 (2005).

²A. Khitun, M. Bao, and K. L. Wang, *J. Phys. D* **43**, 264005 (2010).

³Y. Kajiwara, K. Harii, S. Takahashi, J. Ohe, K. Uchida, M. Mizuguchi, H. Umezawa, H. Kawai, K. Ando, K. Takanashi *et al.*, *Nature (London)* **464**, 262 (2010).

⁴I. Žutić, J. Fabian, and S. Das Sarma, *Rev. Mod. Phys.* **76**, 323 (2004).

⁵V. V. Kruglyak, S. O. Demokritov, and D. Grundler, *J. Phys. D* **43**, 264001 (2010).

⁶L. D. Landau, *J. Phys. USSR* **10**, 25 (1946).

⁷Y. Zhang, T.-H. Chuang, K. Zakeri, and J. Kirschner, *Phys. Rev. Lett.* **109**, 087203 (2012).

⁸T. Sebastian, Y. Ohdaira, T. Kubota, P. Pirro, T. Bracher, K. Vogt, A. Serga, H. Naganuma, M. Oogane, Y. Ando *et al.*, *Appl. Phys. Lett.* **100**, 112402 (2012).

⁹R. A. de Groot, F. M. Mueller, P. G. van Engen, and K. H. J. Buschow, *Phys. Rev. Lett.* **50**, 2024 (1983).

¹⁰P. Buczek, A. Ernst, P. Bruno, and L. M. Sandratskii, *Phys. Rev. Lett.* **102**, 247206 (2009).

¹¹T. Satoh, SPIE Newsroom, doi: 10.1117/2.1201212.004631 (2013).

¹²J. Nishitani, T. Nagashima, and M. Hangyo, *Phys. Rev. B* **85**, 174439 (2012).

¹³T. Satoh, Y. Terui, R. Moriya, B. A. Ivanov, K. Ando, E. Saitoh, T. Shimura, and K. Kuroda, *Nat. Photon.* **6**, 662 (2012).

¹⁴R. A. de Groot, *Physica B: Condens. Matter* **172**, 45 (1991).

¹⁵X. Hu, *Adv. Mater.* **24**, 294 (2012).

¹⁶E. Şaşıoğlu, *Phys. Rev. B* **79**, 100406 (2009).

¹⁷L. M. Sandratskii and P. Buczek, *Phys. Rev. B* **85**, 020406 (2012).

¹⁸E. K. U. Gross and W. Kohn, *Phys. Rev. Lett.* **55**, 2850 (1985).

¹⁹P. Buczek, A. Ernst, and L. M. Sandratskii, *Phys. Rev. B* **84**, 174418 (2011).

²⁰J. Callaway and C. S. Wang, *J. Phys. F: Met. Phys.* **5**, 2119 (1975).

²¹A. Liechtenstein, M. Katsnelson, and V. Gubanov, *J. Phys. F: Met. Phys.* **14**, L125 (1984).

²²A. I. Liechtenstein, M. I. Katsnelson, V. P. Antropov, and V. A. Gubanov, *J. Magn. Magn. Mater.* **67**, 65 (1987).

²³N. Papanikolaou, R. Zeller, and P. H. Dederichs, *J. Phys.: Condens. Matter* **14**, 2799 (2002).

²⁴We used as lattice constant 11.34 atomic units.

²⁵C. Kittel, *Introduction to Solid State Physics* (Wiley, New York, 2005).

²⁶F. Keffer, H. Kaplan, and Y. Yafet, *Am. J. Phys.* **21**, 250 (1953).

²⁷P. Bruno, *Phys. Rev. Lett.* **90**, 087205 (2003).